Stem Cell Reports

Article

ISSCR

OPEN ACCESS

Patient-specific iPSC-derived endothelial cells reveal aberrant p38 MAPK signaling in atypical hemolytic uremic syndrome

Danni Zhou,[1,4,5,15] Ying Tan,[2,6,7,8,15] Xiaoling Liu,[2,6,7,8] Ling Tang,[1,4,5] Hao Wang,[11,12] Jiaxi Shen,[1,4,5] Wei Wang,[13] Lenan Zhuang,[14] Juan Tao,[2,6,7,8] Jun Su,[1,4,5] Tingyu Gong,[1] Xiaorong Liu,[3,*] Ping Liang,[1,4,5,*] Feng Yu,[2,6,7,8,9,*] and Minghui Zhao[2,6,7,8,10]

[1]Division of Hepatobiliary and Pancreatic Surgery, The First Affiliated Hospital, Zhejiang University School of Medicine, 79 Qingchun Road, Hangzhou 310003, China
[2]Renal Division, Department of Medicine, Peking University First Hospital, 8 Xishiku Street, Beijing 100034, China
[3]Department of Nephrology, Beijing Children's Hospital affiliated with Capital Medical University, 56 Nanlishi Road, Beijing 100045, China
[4]NHC Key Laboratory of Combined Multi-organ Transplantation, Hangzhou 310003, China
[5]Institute of Translational Medicine, Zhejiang University, Hangzhou 310029, China
[6]Peking University Institute of Nephrology, Beijing 100034, China
[7]Key Laboratory of Renal Disease, Ministry of Health of China, Beijing 100034, China
[8]Key Laboratory of Chronic Kidney Disease Prevention and Treatment, Ministry of Education of China, Beijing 100034, China
[9]Department of Nephrology, Peking University International Hospital, Beijing 102206, China
[10]Peking-Tsinghua Center for Life Sciences, Peking University, Beijing 100034, China
[11]Department of Prenatal Diagnosis (Screening) Center, Hangzhou Women's Hospital (Hangzhou Maternity and Child Health Care Hospital), Hangzhou 310008, China
[12]Department of Cell Biology and Medical Genetics, Zhejiang University School of Medicine, Hangzhou 310058, China
[13]Department of Cardiology, the Children's Hospital, Zhejiang University School of Medicine, Hangzhou 310003, China
[14]Department of Veterinary Medicine, College of Animal Sciences, Zhejiang University, Hangzhou 310058, China
[15]These authors contributed equally
*Correspondence: lxrbch@sina.com (X.L.), pingliang@zju.edu.cn (P.L.), yufengevert1@sina.com (F.Y.)
https://doi.org/10.1016/j.stemcr.2021.07.011

SUMMARY

Atypical hemolytic uremic syndrome (aHUS) is a rare disease associated with high morbidity and mortality. Existing evidence suggests that the central pathogenesis to aHUS might be endothelial cell damage. Nevertheless, the role of endothelial cell alterations in aHUS has not been well characterized and the underlying mechanisms remain unclear. Utilizing an induced pluripotent stem cell-derived endothelial cell (iPSC-EC) model, we showed that anti-complement factor H autoantibody-associated aHUS patient-specific iPSC-ECs exhibited an intrinsic defect in endothelial functions. Stimulation using aHUS serums exacerbated endothelial dysfunctions, leading to cell apoptosis in iPSC-ECs. Importantly, we identified p38 as a novel signaling pathway contributing to endothelial dysfunctions in aHUS. These results illustrate that iPSC-ECs can be a reliable model to recapitulate EC pathological features, thus providing a unique platform for gaining mechanistic insights into EC injury in aHUS. Our findings highlight that the p38 MAPK signaling pathway can be a therapeutic target for treatment of aHUS.

INTRODUCTION

Atypical hemolytic uremic syndrome (aHUS) is a rare and life-threatening disease characterized by microvascular hemolytic anemia, thrombocytopenia, and acute renal failure (Hofer et al., 2014). After the appearance of initial clinical symptoms, 33%–40% of aHUS patients progress to death or end-stage renal disease (Caprioli et al., 2006; Noris et al., 2010). Within 1 year after diagnosis, 65% of the patients may progress to death, need dialysis, or have permanent renal injury, whether or not they have plasma exchange or infusion (Caprioli et al., 2006).

The majority of aHUS patients carry genetic mutations predisposed for defective complement regulation, which can be subdivided into loss of function mutations of complement regulators (e.g., complement factor H [CFH], complement factor H-related proteins [CFHRs], membrane cofactor protein, complement factor I) and gain-of-function mutations of complement activators (e.g., comple-

ment factor B, C3) (Feitz et al., 2018; Raina et al., 2019). In addition to genetic defects, acquired deficiency in CFH function can result from anti-CFH autoantibodies that are usually associated with the occurrence of a homozygous deletion in CFHR1 and CFHR3 (Dragon-Durey et al., 2010; Józsi et al., 2008; Song et al., 2017). Our previous studies suggest that the properties of CFH antibodies can influence and impair the biological role of CFH and therefore contribute to aHUS susceptibility (Guo et al., 2019). However, some patients with anti-CFH autoantibodies, even with the epitope on short consensus repeats 15–20, showed no sign of aHUS (Seikrit et al., 2018).

EC injury is the central event in the pathophysiology of aHUS due to uncontrolled complement overactivation. Physiologically, CFH regulates the alternative pathway of complement activation to prevent self-damage. In anti-CFH autoantibody-associated aHUS, genetic defects or anti-CFH autoantibodies result in long-term, chronic, and uncontrolled complement activation and accumulation

of membrane attack complex (MAC), which lead to damage of the global ECs, cell swelling, and inflammation (Durey et al., 2016; Puraswani et al., 2019). Existing studies have also found that certain mutations such as DGKE may cause impaired EC repair and angiogenesis *in vivo* (Bruneau et al., 2015).

The discovery of induced pluripotent stem cells (iPSCs) offers a new paradigm for the study of human diseases (Takahashi et al., 2007). The advantages of iPSCs include their patient origin, easy accessibility, expandability, ability to give rise to almost all types of cells desired, avoidance of ethical concerns associated with human embryonic stem cells (hESCs), and the potential to develop personalized medicine (Shi et al., 2017). Patient- and disease-specific iPSC-derived endothelial cells (iPSC-ECs) have been utilized for studying disease mechanisms underlying endothelial dysfunction including pulmonary arterial hypertension, moyamoya disease, fibrodysplasia ossificans progressiva, Kawasaki disease, Huntington's disease, diabetes mellitus, and hemophilia A (Barruet et al., 2016; Gu et al., 2017; Hamauchi et al., 2016; Hitomi et al., 2013; Ikeda et al., 2016; Lim et al., 2017; Ong et al., 2019; Sa et al., 2017).

In this study, we generated iPSC-ECs from pediatric patients with anti-CFH autoantibody-associated aHUS carrying CFHR1/3 deletions or not as well as healthy control subjects. We investigated whether endothelial dysfunction in aHUS can be recapitulated in patient-specific iPSC-ECs and elucidated the underlying mechanism at the cellular level.

RESULTS

Clinical characteristics

We recruited three patients with anti-CFH autoantibody-associated aHUS and two healthy control subjects. The patients were all male teenagers with microangiopathic hemolysis, thrombocytopenia, and acute renal impairment. All of the patients showed positive anti-CFH autoantibodies and hypocomplementemia, especially low levels of CFH. Among the patients, genetic screening revealed that the first patient (aHUS#1) was homozygous for a CFHR1 deletion and heterozygous for a CFHR3 deletion; the second patient (aHUS#2) was homozygous for both a CFHR1 deletion and a CFHR3 deletion; no CFHR1/CFHR3 deletions or mutations were detected in the third patient (aHUS#3) (Table S1). The relative optical density (OD) values of the anti-CFH autoantibodies for the three aHUS patients in active phase were 0.87, 0.89, and 1.95, respectively (cutoff OD: 0.20). The detailed clinical and laboratory data of the recruited aHUS patients are provided in Table S1. Our two healthy control subjects were a 9-year-

old boy and a 10-year-old boy with no history of renal disease, hemolytic anemia, or thrombocytopenia.

Generation and characterization of patient-specific aHUS iPSCs

Skin biopsies were obtained from the recruited healthy control subjects and aHUS patients, and skin fibroblasts were cultured and expanded (Figure 1A and Table S2). iPSCs were then generated from primary fibroblasts by using non-integrated Sendai-viral transduction of the reprogramming factors (Oct3/4, Sox-2, Klf-4, and c-Myc). Control and aHUS iPSC lines showed typical hESC morphology (Figure 1B) and normal karyotype (Figure 1C). Generated iPSCs also displayed alkaline phosphatase activity (Figure 1D), stained positive for pluripotent markers including OCT4, SOX2, NANOG, and SSEA4 (Figures 1E and 1F), and expressed pluripotency genes SOX2 and OCT4 (Figures S1A and S1B; Table S3). In addition, teratoma formation assays using control and aHUS iPSCs produced derivatives from all three germ layers (Figures S1C and S1D). At least two iPSC lines were generated from each individual and were used for downstream characterization.

Generation and characterization of ECs derived from patient-specific aHUS iPSCs

Using an *in vitro* monolayer endothelial differentiation protocol, we successfully differentiated control and aHUS iPSCs into ECs (Figure 2A). On day 10 of induction of differentiation, we observed dramatic morphological change toward ECs (Figure 2B). CD144 positive cells were subsequently sorted by magnetic-activated cell sorting (MACS) and plated on 0.2% gelatin-coated plates for downstream expansion and characterization. Both control and aHUS iPSC-ECs exhibited positive staining of endothelial-specific marker CD144 as well as Dil-LDL uptake (Figures 2C and 2D).

Endothelial dysfunction phenotypes in aHUS iPSC-ECs

EC injury is central to the pathogenesis of aHUS (Noris and Remuzzi, 2005). We therefore investigated whether aHUS patient-specific iPSC-ECs could recapitulate functional phenotypes under baseline conditions. aHUS iPSC-ECs showed decreased migration detected by a wound closure scratch assay as compared with control iPSC-ECs (control: 67.3% ± 4.2%; aHUS: 28.3% ± 2.0%) (Figures 3A and 3B). Moreover, aHUS iPSC-ECs exhibited significantly decreased tube formation capacity compared with control iPSC-ECs, with reduced numbers of tube-like structures (control: 43 ± 3; aHUS: 32 ± 1) as well as reduced tube length (control: 10,368 ± 563.6 μm; aHUS: 6,689 ± 314.9 μm) (Figures 3C–3E). We also observed impaired cell proliferation in aHUS iPSC-ECs when compared with
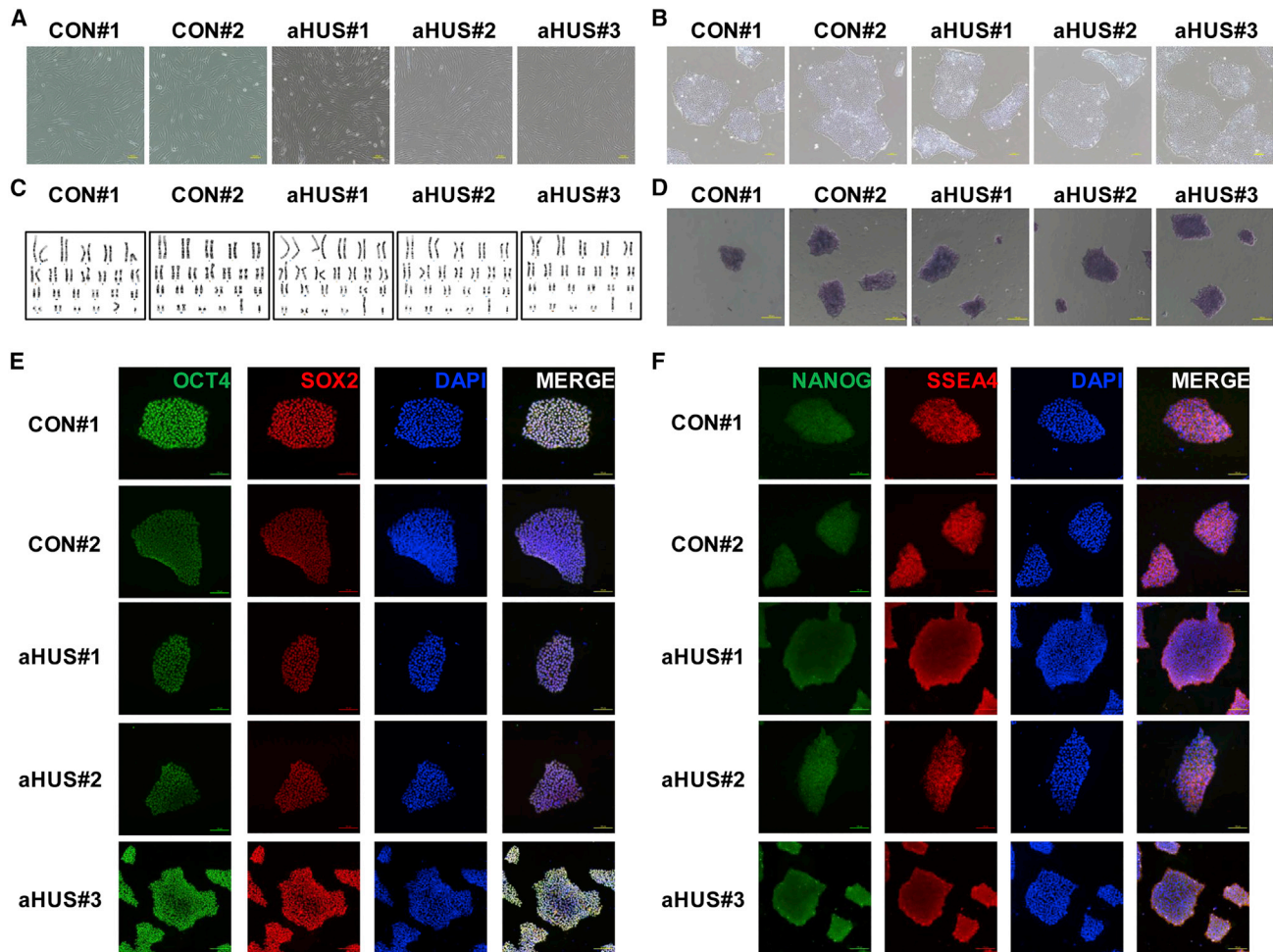
Figure 1. Generation and characterization of patient-specific aHUS iPSCs

(A) Typical morphology of skin fibroblasts derived from three pediatric patients with anti-CFH autoantibody-associated aHUS and two healthy control subjects (shown as CON). Scale bars, 100 μm.

(B) Typical morphology of iPSC colony derived from control and aHUS skin fibroblasts. Scale bars, 100 μm.

(C) Karyotype analysis of control and aHUS iPSCs.

(D) Alkaline phosphatase staining of control and aHUS iPSCs. Scale bars, 50 μm.

(E and F) Pluripotent staining of control and aHUS iPSCs using OCT4 (green), SOX2 (red), NANOG (green), and SSEA4 (red). DAPI indicates nuclear staining (blue). Scale bars, 100 μm.

control cells (Figure 3F). Taken together, these results demonstrate that aHUS patient-specific iPSC-ECs exhibit abnormal endothelial function compared with control iPSC-ECs.

aHUS serum stimulation exacerbates EC function and induces EC apoptosis

Accumulating studies have suggested the pathogenic role of anti-CFH autoantibodies in aHUS (Blanc et al., 2012; Jozsi et al., 2007; Strobel et al., 2010, 2011). We next sought to investigate whether aHUS serum containing anti-CFH autoantibodies has functional effects on EC function. We observed no significant change of EC function in control

or aHUS iPSC-ECs upon stimulation of the normal serum from healthy control subjects (Figures 4A–4E). In contrast, after stimulation of the diseased serum from aHUS#1 or aHUS#2, the cell migration and tube formation capacities were greatly impaired in both control and aHUS iPSC-ECs (Figures 4A–4E). Moreover, we observed significantly reduced cell viability as detected by CCK-8 (Cell Counting Kit-8) assay in both control and aHUS iPSC-ECs after diseased serum stimulation when compared with basal or normal serum-stimulated condition (Figure 4F). We next performed a TUNEL (terminal deoxynucleotidyl transferase-mediated deoxyuridine triphosphate nick end labeling) assay to assess whether the cell loss was associated with
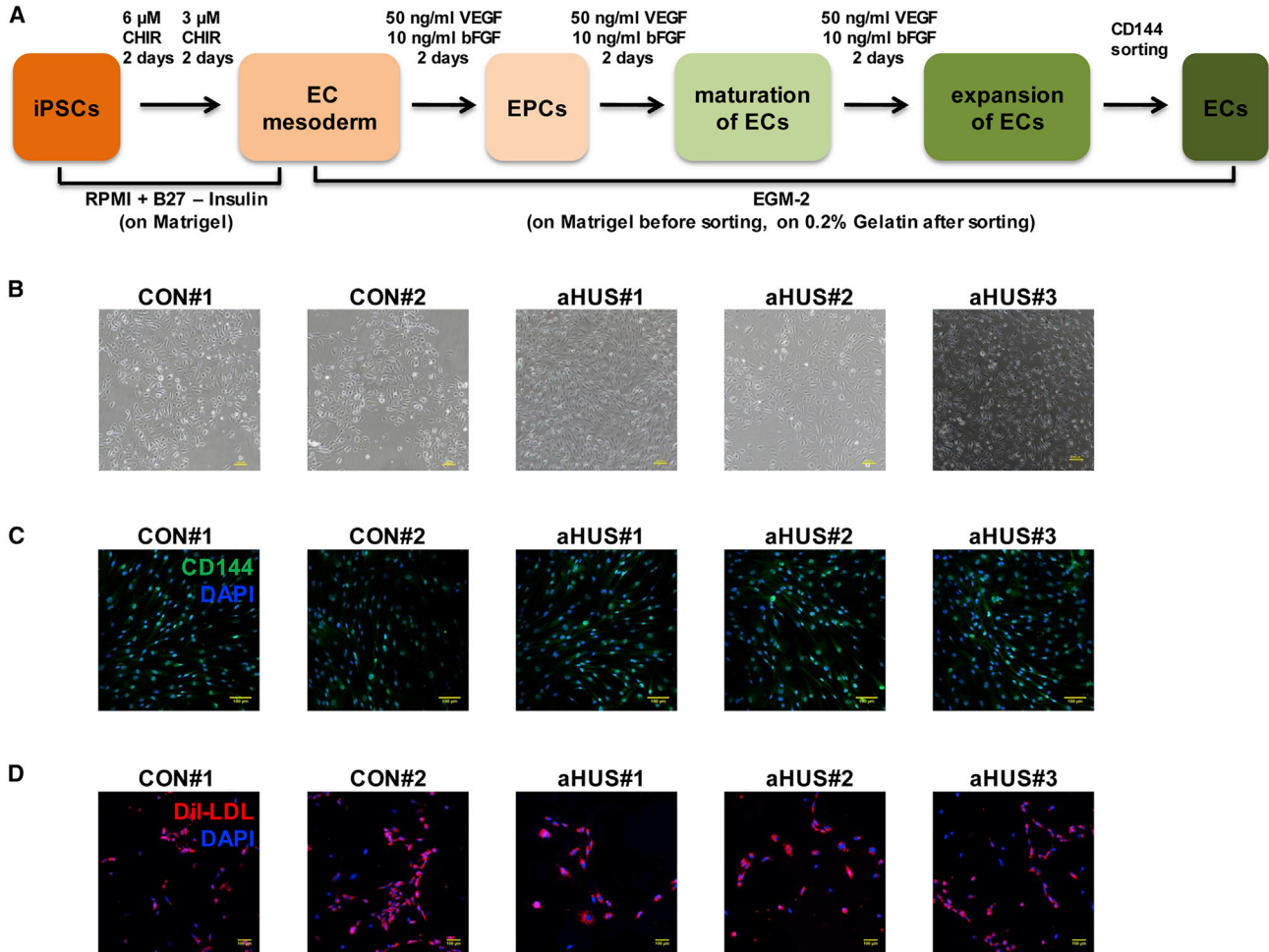
Figure 2. Generation and characterization of endothelial cells derived from patient-specific aHUS iPSCs

(A) Schematic demonstration of iPSC-derived endothelial cell (EC) differentiation. CHIR, CHIR-99021; VEGF, vascular endothelial growth factor; bFGF, basic fibroblast growth factor; EPCs, endothelial progenitor cells.

(B) Typical morphology of control and aHUS iPSC-ECs. Scale bars, 100 μm.

(C) CD144 (green) staining of control and aHUS iPSC-ECs. DAPI indicates nuclear staining (blue). Scale bars, 50 μm.

(D) Dil-LDL (red) staining of control and aHUS iPSC-ECs. DAPI indicates nuclear staining (blue). Scale bars, 100 μm.

apoptosis. We observed a significantly increased ratio of TUNEL-positive cells in both control and aHUS iPSC-ECs stimulated by diseased serum, whereas normal serum had no effect on EC apoptosis (Figure S2). Consistent with the TUNEL results, the expression of caspase-3 was significantly increased in both control and aHUS iPSC-ECs after diseased serum stimulation (Figure S3). Interestingly, treatment with a complement inhibitor, compstatin (50 μM, 2 days), in aHUS-diseased serum-treated iPSC-ECs significantly rescued the endothelial dysfunction and apoptosis phenotypes and restored the cell viability (Figures 4A–4F and S2). Collectively, these results suggest that complement activation may play an important role in the effects of diseased serum derived from aHUS

patients in exacerbating EC dysfunction and inducing EC apoptosis.

Anti-CFH autoantibodies alone have no effects on EC loss

Successful purification of anti-CFH autoantibodies from two recruited aHUS patients allowed us to test whether anti-CFH autoantibodies could directly cause EC loss. iPSC-ECs were treated under the following conditions for 2 days: (1) normal immunoglobulin G (IgG) alone; (2) normal IgG plus normal serum; (3) normal IgG plus denatured normal serum (boiled at 56°C for 30 min); (4) normal IgG plus normal serum plus compstatin; (5) anti-CFH autoantibodies alone; (6) anti-CFH autoantibody plus normal

Figure 3. Endothelial dysfunction phenotype in aHUS iPSC-ECs

(A) Representative images of wound closure in control and aHUS iPSC-ECs assessed at 12 h. Scale bars, 100 μm.

(B) Scatterplot to compare the percentage of wound closure between control and aHUS iPSC-ECs. ****p < 0.0001; n = 8 independent experiments.

(C) Representative images of tube formation on Matrigel in control and aHUS iPSC-ECs assessed at 6 h. Scale bars, 100 μm.

(D and E) Scatterplots to compare the number of tube-like structures (D) or tube length (E) between control and aHUS iPSC-ECs. ***p < 0.001, ****p < 0.0001; n = 8 independent experiments.

(F) Scatterplot to compare the cell proliferation between control and aHUS iPSC-ECs using absorbance reads at 450 nm. ***p < 0.001; n = 8 independent experiments.

serum; (7) anti-CFH autoantibody plus denatured normal serum; (8) anti-CFH autoantibody plus normal serum plus compstatin. We observed comparable CCK-8 or TUNEL signal in both control and aHUS iPSC-ECs between basal, normal IgG alone, normal IgG plus normal serum, and normal IgG plus denatured normal serum conditions (Figures S4 and S5). Moreover, stimulation of anti-CFH autoantibodies alone showed no significant change of cell viability or apoptosis in control and aHUS iPSC-ECs. Notably, anti-CFH autoantibodies, when combined with normal serum, resulted in greatly increased cell death as detected by CCK-8 or TUNEL assay, which can be effectively rescued by denaturation of the serum and treatment with

compstatin (Figures S4 and S5). Taken together, these results suggest that anti-CFH autoantibodies alone have no effects on EC loss.

RNA-sequencing analysis of aHUS iPSC-ECs

To further investigate the molecular mechanisms of EC dysfunction phenotype in aHUS, we next performed genome-wide RNA sequencing (RNA-seq) by comparing control and aHUS iPSC-ECs. We observed that 1,401 genes out of a total of 12,045 genes were differentially expressed in aHUS iPSC-ECs as compared with control iPSC-ECs, in which 659 were upregulated and 742 were downregulated (Figures 5A–5C). Gene ontology (GO) analysis revealed
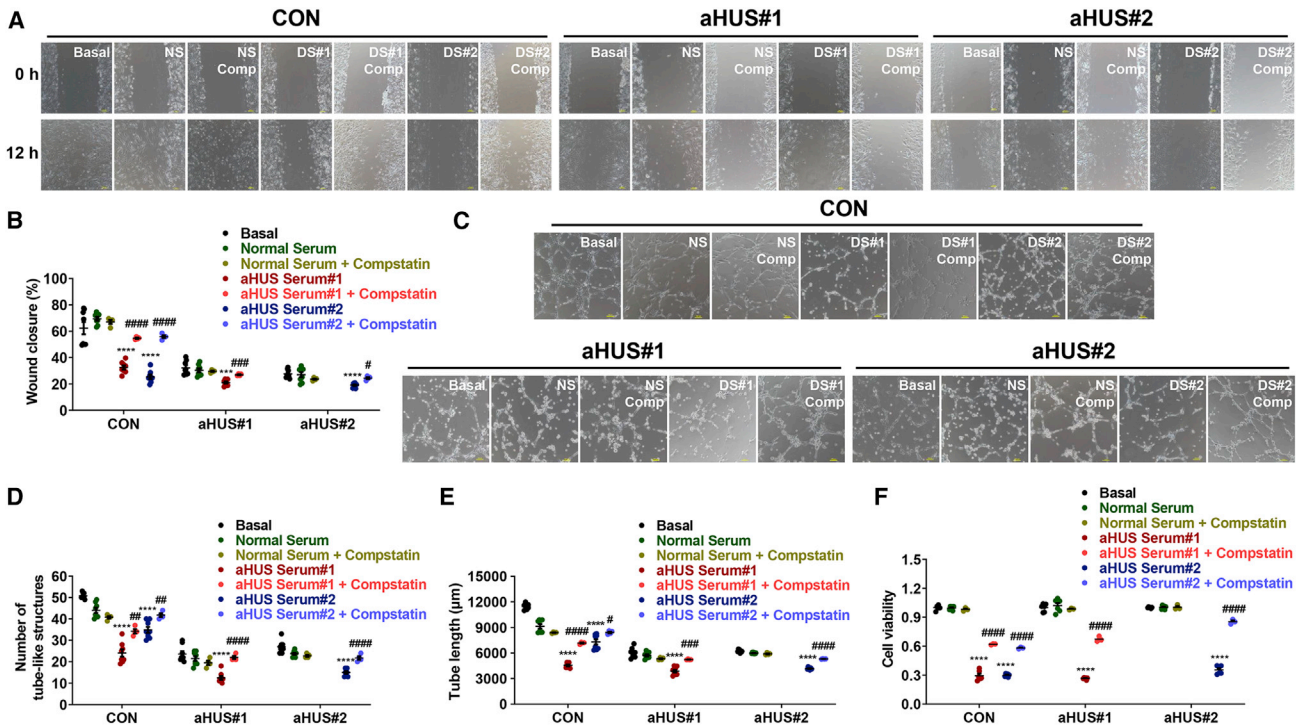
Figure 4. aHUS serum stimulation exacerbates EC function and induces EC loss

(A) Representative images of wound closure in control and aHUS iPSC-ECs under different conditions, including basal, normal or aHUS-diseased serum alone (NS or DS), and normal or aHUS-diseased serum plus compstatin (NS Comp or DS Comp). Scale bars, 100 μm.

(B) Scatterplot to compare the percentage of wound closure between different groups. ***$p < 0.001$ and ****$p < 0.0001$, compared with basal; [#]$p < 0.05$, [###]$p < 0.001$, and [####]$p < 0.0001$, compared with serum alone. n = 4–8 independent experiments.

(C) Representative images of tube formation on Matrigel in control and aHUS iPSC-ECs under basal, normal serum, and aHUS serum stimulation conditions. Scale bars, 100 μm.

(D–F) Scatterplots to compare the number of tube-like structures (D), tube length (E), or cell viability (F) between different groups. ****$p < 0.0001$, compared with basal; [#]$p < 0.05$, [##]$p < 0.01$, [###]$p < 0.001$, and [####]$p < 0.0001$, compared with serum alone. n = 4–8 independent experiments.

that upregulated genes were enriched in "cell cycle," "nuclear division," "organelle fission," "chromosome segregation," and "cell division" (Figure 5D). Downregulated genes were enriched in "blood vessel development," "regulation of proliferation," "blood vessel morphogenesis," "kidney development," "cell migration," and "angiogenesis" (Figures 5E and S6). Interestingly, among the 405 downregulated genes, several important genes, such as PECAM1, BMP4, and HOXA3, were enriched in the "angiogenesis" term of GO analysis (Figures 5F and S6). PECAM1, also known as CD31, plays a vital role in EC migration, cell survival, organization of EC junctions, and maintenance of the EC permeability barrier (Lertkiatmongkol et al., 2016). Bone morphogenetic protein (BMP) signaling affects EC behavior in both pro- and anti-angiogenic ways, and BMP4 regulates pro-angiogenic activity via vascular endothelial growth factor receptor 2 (VEGFR2) (Rezzola et al., 2019). In addition, CDH5 (also known as VE-cadherin or CD144) was significantly downregulated in aHUS iPSC-

ECs, which functions in EC adhesion and plays a key role in EC integrity and vascular homeostasis (Figure 5F) (Giannotta et al., 2013). The mRNA-level expression of *PECAM1*, *BMP4*, *HOXA3*, and *CDH5* was validated by quantitative real-time PCR (qPCR), which was consistent with the RNA-seq data (Figure 5G and Table S3).

Impaired p38 MAPK signaling in aHUS iPSC-ECs

The p38 mitogen-activated protein kinase (MAPK) cascades are major signaling pathways that regulate multiple endothelial functions in response to exogenous and endogenous stimuli including growth factors, stress, and cytokines. In addition, the activation of p38 in ECs leads to actin remodeling, angiogenesis, and DNA damage response, and thereby has a major impact on cardiovascular homeostasis (Corre et al., 2017). It has been shown that p38 can maintain VE-cadherin expression to impede the induction of epithelial-mesenchymal transition in human primary mesothelial cells (Strippoli et al., 2010).
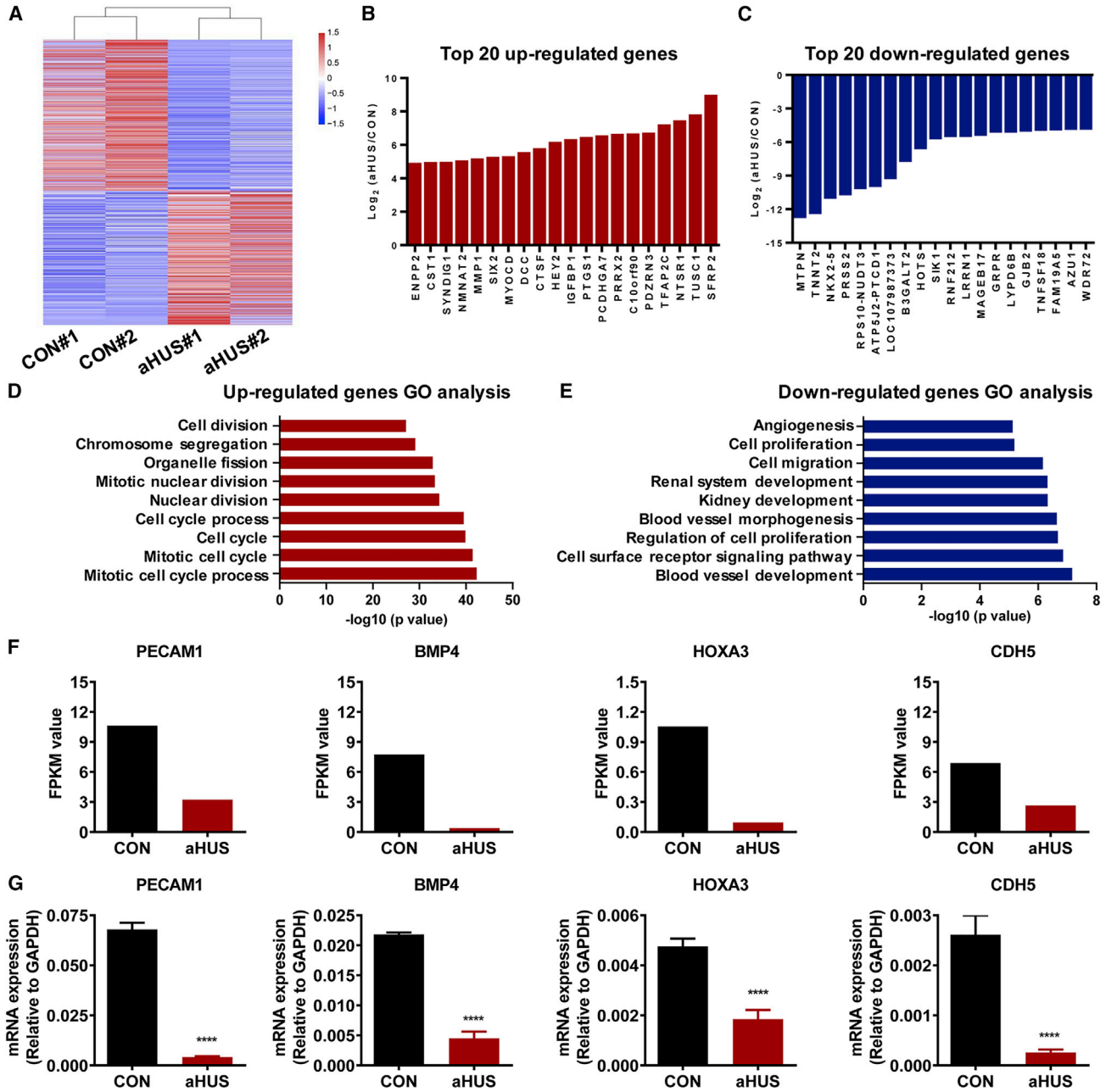
Figure 5. RNA-seq analysis of aHUS iPSC-ECs

(A) Heatmap demonstrating the differential gene expression between control and aHUS iPSC-ECs.

(B and C) Top 20 genes showing the greatest differences in expression between control and aHUS iPSC-ECs, respectively.

(D and E) Gene ontology (GO) analysis using upregulated (D) and downregulated (E) genes.

(F) Bar graphs to compare the FPKM values of *PECAM1*, *BMP4*, *HOXA3*, and *CDH5* between control and aHUS iPSC-ECs.

(G) Bar graphs to compare the mRNA expression of *PECAM1*, *BMP4*, *HOXA3*, and *CDH5* between control and aHUS iPSC-ECs by qPCR. ****p < 0.0001.

In addition, BMP4 stimulates osteocalcin synthesis via p38 in osteoblast-like MC3TS-E1 cells. In the epithelial and mesenchymal tissue compartments of the developing mouse ureter, BMP4 uses several different effector pathways to regulate proliferation and differentiation including the p38 signaling pathways (Kuroyanagi et al., 2015; Mamo et al., 2017). Given that VE-cadherin and BMP4 were significantly downregulated in aHUS iPSC-ECs, we hypothesized
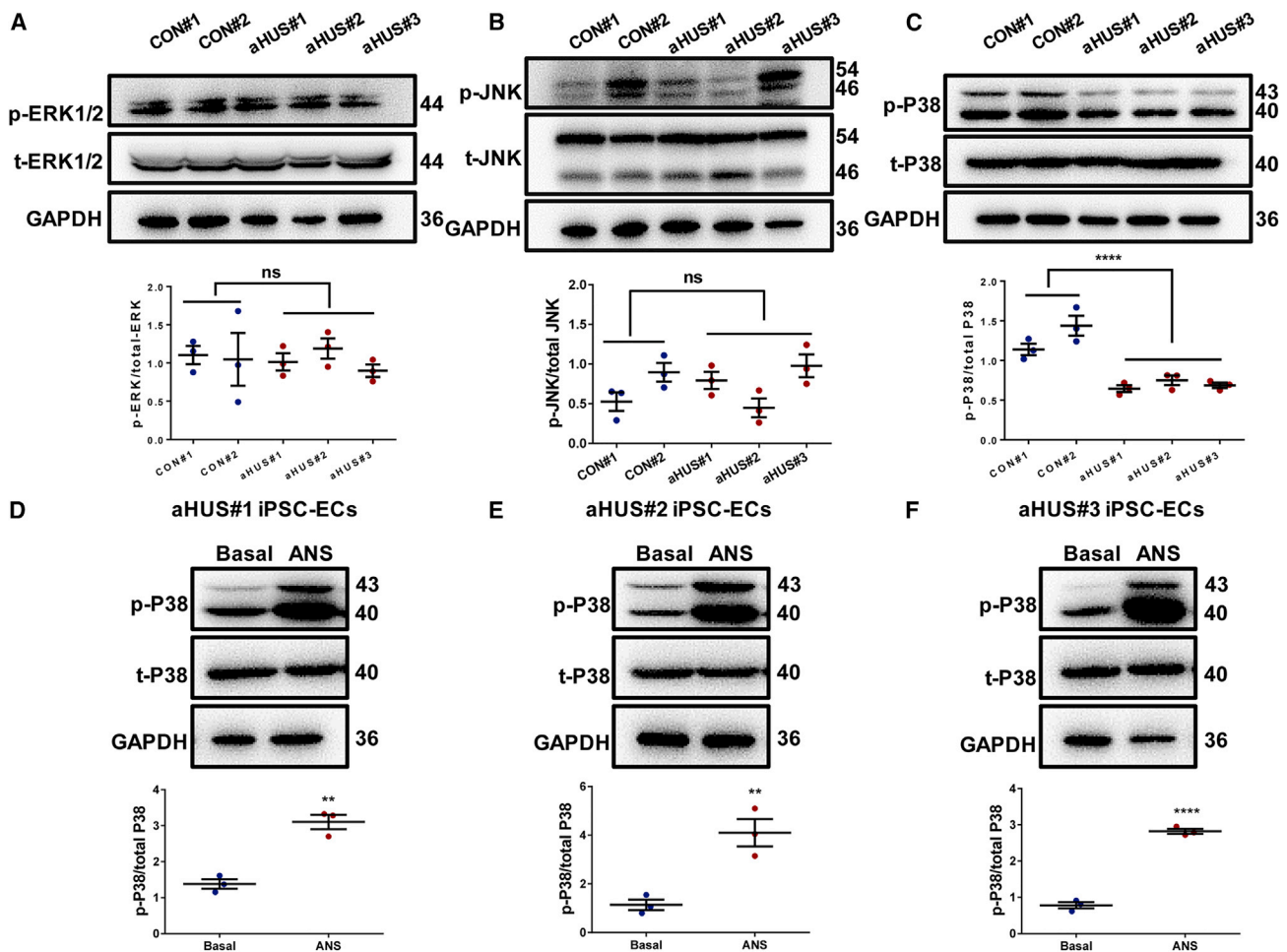
Figure 6. Impaired p38 MAPK signaling in aHUS iPSC-ECs

(A–C) Upper panels: western blot analysis of p-ERK (A), p-JNK (B), or p-p38 (C) expression in control and aHUS iPSC-ECs. Lower panel: scatterplot to compare the p-ERK (A), p-JNK (B), or p-p38 (C) expression between control and aHUS iPSC-ECs. ****p < 0.0001; n = 3 independent EC differentiation experiments.

(D–F) Upper panels: western blot analysis of p-p38 expression in aHUS iPSC-ECs derived from patient #1 (D), patient #2 (E), and patient #3 (F) upon basal or anisomycin (ANS) treatment, respectively. Lower panels: scatterplots to compare the p-p38 expression between basal and ANS-treated aHUS iPSC-ECs. **p < 0.01 and ****p < 0.0001; n = 3 independent experiments.

that p38 signaling pathway may change, thus giving rise to the deleterious phenotypes seen in the diseased cells. To test this notion, we focused on the MAPK signaling pathway which consists of extracellular signal-regulated kinases (ERK), p38, and c-Jun N-terminal kinases (JNK). We performed western blot analysis to assess the expression of phosphorylated ERK1/2 (p-ERK1/2), phosphorylated JNK (p-JNK), and phosphorylated p38 (p-p38) at the protein level in control and aHUS iPSC-ECs. The expression levels of p-ERK and p-JNK remained unchanged between control and aHUS iPSC-ECs (Figures 6A and 6B). However, the expression of p-p38 was significantly decreased in iPSC-ECs from all three aHUS patients compared with control cells (Figure 6C). Importantly, addition of anisomycin

(ANS), a p38-specific activator, effectively restored the expression of p-p38 in aHUS iPSC-ECs (Figures 6D–6F).

Rescuing endothelial phenotypes of aHUS iPSC-ECs by targeting p38 signaling

Consistently, the endothelial dysfunction phenotypes seen in aHUS iPSC-ECs were significantly rescued by ANS to activation of p38 signaling with restored migration (Figures 7A and 7B) and tube formation capacities (Figures 7C–7E). Moreover, overexpression of MKK6, the upstream kinase to activate p38 signaling, significantly increased p-p38 (Figure S7) and largely improved the migration and tube formation capacities in aHUS iPSC-ECs (Figures 7F–7J). Altogether, these results suggest that an aberrant p38
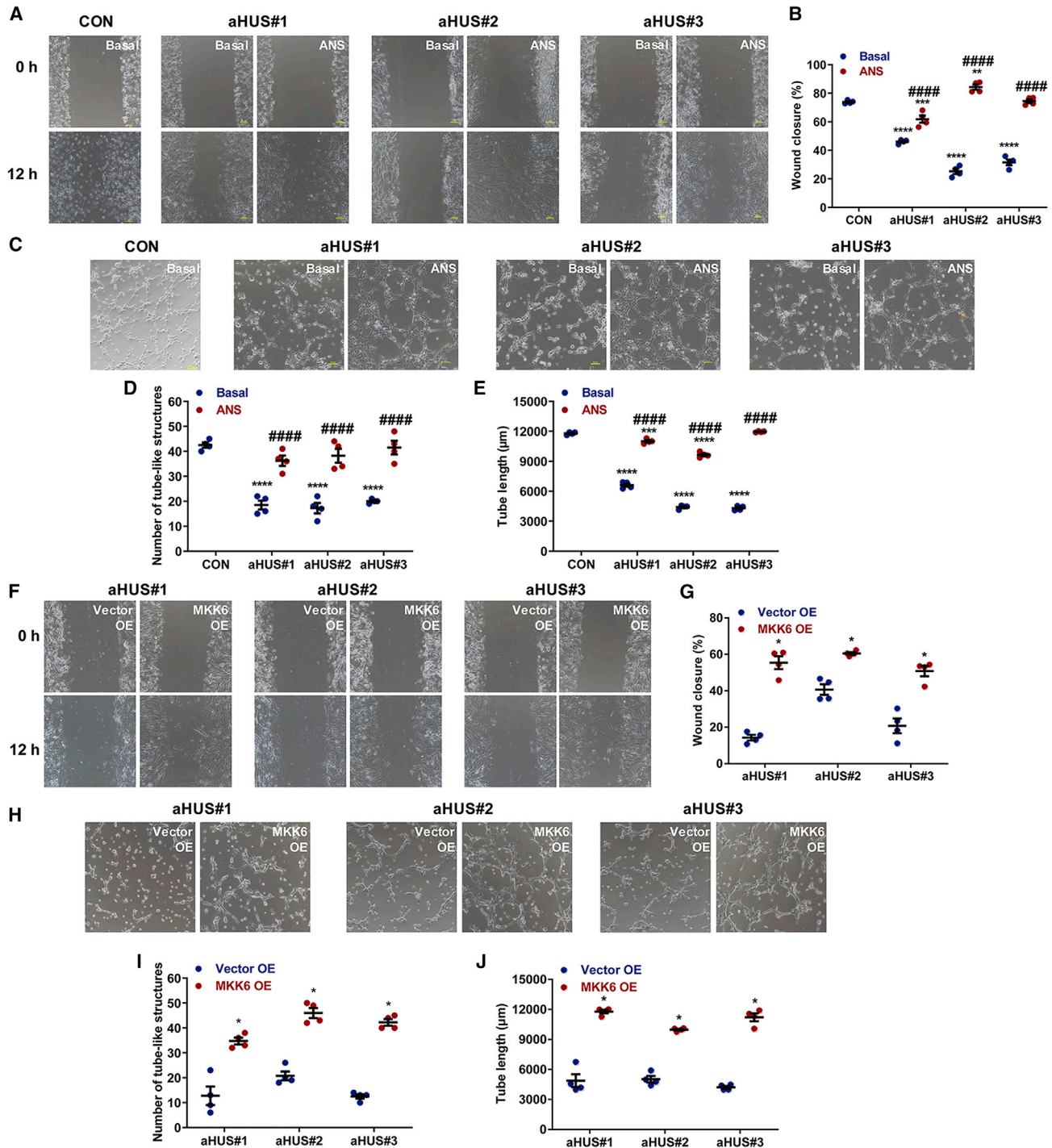
Figure 7. Activation of p38 by anisomycin or MKK6 overexpression rescues endothelial phenotype in aHUS iPSC-ECs

(A) Representative images of wound closure in basal control iPSC-ECs, basal or anisomycin (ANS)-treated aHUS iPSC-ECs. Scale bars, 100 μm.

(B) Scatterplot to compare the percentage of wound closure between different groups. **p < 0.01, ***p < 0.001, and ****p < 0.0001, compared with basal control iPSC-ECs; ####p < 0.0001, compared with basal aHUS iPSC-ECs. n = 4 independent experiments.

(C) Representative images of tube formation on Matrigel in basal control iPSC-ECs, basal, or ANS-treated aHUS iPSC-ECs. Scale bars, 100 μm.

(legend continued on next page)

signaling, as a common signature pathway in anti-CFH autoantibody-associated aHUS, may contribute to the endothelial dysfunction phenotypes.

DISCUSSION

Here, we utilized a human iPSC-EC platform to elucidate the molecular mechanisms underlying the endothelial dysfunction phenotypes observed in aHUS patients.

aHUS is a persistent disease associated with high morbidity and mortality. The molecular mechanisms underpinning the development of aHUS remain largely unknown. Experimental mouse models have been used to understand the functional changes of genetic mutations identified in aHUS patients (de Jorge et al., 2011; Smith-Jackson et al., 2019; Ueda et al., 2017). However, mouse models do not always demonstrate the same phenotypes as those observed in humans, thus reducing the clinical relevance of observations in mouse models. Our study, for the first time, provided a human-based "disease in a dish" model to gain mechanistic insights of endothelial dysfunction related to aHUS in a native cellular context.

The main pathological feature of aHUS is EC injury, which is characterized by thickening of arterioles and capillaries, endothelial swelling and detachment, thrombosis, and obstruction of the vessel lumina. Lesions typically affect the kidney, but the brain, heart, lungs, eyes, gastrointestinal tract, liver, and pancreas might also be involved (Loirat et al., 2008; Noris and Remuzzi, 2009). However, a comprehensive characterization of endothelial function in aHUS has not been performed. In this study, we recruited three aHUS pediatric patients, all having anti-CFH autoantibodies. Multiple iPSC lines were generated from aHUS patients and age- and gender-matched healthy control subjects by reprogramming skin fibroblasts, and iPSC-ECs were successfully differentiated and functionally characterized. Surprisingly, the seminal finding in our study is that there is a global impairment of endothelial functions in aHUS iPSC-ECs at baseline condition, although there is no significant change in cell apoptosis between control and aHUS iPSC-ECs. We find that aHUS patient-specific iPSC-ECs exhibited dysfunctional endothelial phenotypes, as char-acterized by decreased migration, decreased tube formation capacity, and impaired cell proliferation. Our results suggest that an intrinsic defect in ECs occurs in anti-CFH auto-antibody-associated aHUS.

CFH is frequently targeted in aHUS, which is the main regulatory component of the alternative pathway of complement activation to prevent self-damage (Durey et al., 2016; Loirat and Frémeaux-Bacchi, 2011). Autoantibodies against CFH account for 10% of cases of aHUS, which mainly develop in the context of a homozygous deletion of the genes encoding the CFH-related proteins CFHR1 and CFHR3 (Dragon-Durey et al., 2010; Józsi et al., 2008). Accumulating evidence has suggested the pathogenicity of CFH autoantibodies in aHUS (Blanc et al., 2012; Dragon-Durey et al., 2005; Jozsi et al., 2007; Puraswani et al., 2019; Strobel et al., 2010, 2011). The pathogenesis of anti-CFH autoantibody-associated aHUS was previously thought to be exposure of ECs to overactivation of the alternative complement pathway. EC damage is evident in histologic analysis of renal biopsies taken from aHUS patients during the acute stage, such as EC swelling, subendo-thelial edema, fibrin microthrombus (either in glomeruli or in small arterioles and/or in arteries), mucoid changes, and onion-skin lesions of arterioles and/or arteries. The pathogenicity of anti-CFH autoantibodies has been demonstrated as a deficiency in CFH function *in vitro*. Furthermore, eculizumab, a complement C5-targeting monoclonal antibody that blocks generation of C5a and prevents the assembly of the MAC, showed efficacy in anti-CFH autoantibody-associated aHUS patients (Noone et al., 2014). However, functional consequences of CFH au-toantibodies acting on ECs have not been addressed as yet. We demonstrated that stimulation of aHUS patient-specific serum containing CFH autoantibodies further exacerbated EC dysfunction phenotypes. Moreover, stimulation of aHUS serum resulted in reduced cell viability and apoptosis in both control and aHUS iPSC-ECs, which was not observed under baseline conditions. These results provide functional evidence that the generation of CFH autoanti-bodies is pathogenic and may cause EC injury in aHUS.

aHUS iPSC-ECs displayed dysfunctional phenotypes at baseline compared with control iPSC-ECs, and the diseased serum could exacerbate EC dysfunction and induce

(D and E) Scatterplots to compare the number of tube-like structures (D) or tube length (E) between different groups. ***p < 0.001 and ****p < 0.0001, compared with basal control iPSC-ECs; ####p < 0.0001, compared with basal aHUS iPSC-ECs. n = 4 independent experiments.

(F) Representative images of wound closure in aHUS iPSC-ECs overexpressing vector only (Vector OE) or MKK6 (MKK6 OE). Scale bars, 100 μm.

(G) Scatterplot to compare the percentage of wound closure between different groups. *p < 0.05; n = 4 independent experiments.

(H) Representative images of tube formation on Matrigel in aHUS iPSC-ECs overexpressing vector only or MKK6. Scale bars, 100 μm.

(I and J) Scatterplots to compare the number of tube-like structures (I) or tube length (J) between different groups. *p < 0.05; n = 4 independent experiments.

apoptosis, which supports the "second-hit" hypothesis. The same common variants of rs2498804, rs1800470, and rs1075846 (Chen et al., 2012; McCarthy et al., 2013; Rossi et al., 2013), which were reported to be associated with reduced anti-apoptotic efficiency, increased risk of endothelial diseases, or defective cell migration, shared by all the three patients might explain the endothelial dysfunction at baseline, while the diseased serum including anti-CFH autoantibody and complements should be the add-on "hit" of endothelial dysfunction.

Notably, purified anti-CFH autoantibodies were also assessed in the iPSC-EC model, with no phenotypic change in EC loss. Nevertheless, stimulation of anti-CFH autoantibodies combined with normal serum gave rise to significantly increased EC apoptosis, indicating that auto-antibodies alone may not directly cause EC injury, thus requiring a serum environment leading to EC injury in aHUS. The resulting EC apoptosis phenotype induced by anti-CFH autoantibodies plus normal serum can be rescued by denaturation of the serum or the complement inhibitor (compstatin), which is in agreement with our previous work that the anti-CFH antibodies could bind to CFH and get involved in the dysregulation of the alternative complement pathway (Guo et al., 2019). Moreover, aHUS iPSC-ECs demonstrated a more severe cell apoptosis phenotype upon anti-CFH antibody plus normal serum stimulation as compared with control iPSC-ECs, supporting the "two-hit" model in which the pathogenic role of anti-CFH auto-antibodies and the patients with genetic predisposing background (CFHR1/3 deletions) of endothelial injury result in anti-CFH autoantibody-associated aHUS, as previous studies demonstrated that patients with rheumatoid arthritis, systemic lupus erythematosus, or antiphospholipid syndrome also showed positive anti-CFH autoantibodies but not thrombotic microangiopathy, which might be due to the absence of CFHR1 homozygous deletions or endothelial-associated SNPs.

Generation of a large amount and purified patient-specific iPSC-ECs allowed us to perform accurate RNA-seq analysis and functional validations to search for critical signaling pathways associated with aHUS. Indeed, we identified that p38 MAPK signaling was impaired in diseased iPSC-ECs from all three patients with anti-CFH autoantibody-associated aHUS. It has been widely acknowledged that p38 MAPK is essential for EC function, which is an important therapeutic target in various diseases (Issbrucker et al., 2003; Kim et al., 2012; Kumar et al., 2003; Saklatvala 2004; Tielemans et al., 2019; Yong et al., 2009). Interestingly, a previous study showed that diacylglycerol kinase ε encoded by aHUS-associated gene *DGKE* regulates EC activation through upregulation of p38 MAPK-mediated signals (Bruneau et al., 2015). The discrepancies of p38 signaling changes may arise from distinct mechanisms in different

subtypes of aHUS. Anti-CFH autoantibodies were associated with a deficiency in CFHR1 in over 80% of anti-CFH autoantibody-associated aHUS (Durey et al., 2016). More interestingly, 4 of 21 asymptomatic siblings of patients with anti-CFH autoantibody-associated aHUS had elevated antibody titers and homozygous deletion of CFHR1 but normal urinalysis and preserved kidney function, suggesting that additional factors are required for the onset of the disease (Sinha et al., 2014). Our study firstly demonstrated that patients with or without CHFR1/3 deletion showed endothelial dysfunction and decreased p38 MAPK signaling, which might indicate that CHFR1/3 deletion was not associated with primary endothelial dysfunction and may provide a new explanation of the hereditary susceptibility of the disease onset. Importantly, by both pharmacological agonist and genetic manipulation, we showed that restoration of p38 MAPK signaling effectively rescued abnormal functional phenotypes seen in aHUS iPSC-ECs from all three patients, indicating a common signaling pathway in anti-CFH autoantibody-associated aHUS and thus providing a new target for treatment of the disease.

In conclusion, iPSC-ECs can be a reliable model to recapitulate the EC pathological features, thus providing a unique platform for gaining mechanistic insights of the EC injury in aHUS. Our findings highlighted that the p38 MAPK signaling pathway can be a therapeutic target for treatment of anti-CFH autoantibody-associated aHUS.

EXPERIMENTAL PROCEDURES

Patient recruitment

Skin biopsies were obtained from three patients with anti-CFH autoantibody-associated aHUS and two age- and gender-matched healthy control subjects, who all signed informed consents. This study was approved by the Ethics Committees of Peking University First Hospital and Beijing Children's Hospital.

Skin biopsies and maintenance of fibroblasts

The timing of skin biopsies for the three patients was in remission phase. Freshly isolated skin biopsies were rinsed with Dulbecco's phosphate-buffered saline (DPBS) and transferred into a 1.5-mL tube. Tissue was minced in collagenase I (1 mg/mL in Dulbecco's modified Eagle's medium [DMEM], Gibco) and allowed to digest for 6 h at 37°C. Dissociated dermal fibroblasts were plated and maintained with DMEM containing 10% fetal bovine serum (FBS) (Gibco), Glutamax (Gibco), 4.5 g/L glucose (Gibco), 110 mg/L sodium pyruvate (Gibco), 50 U/mL penicillin (Gibco), and 50 g/mL streptomycin (Gibco) at 37°C, 95% air, and 5% CO_2 in a humidified incubator. All cells were used for reprogramming within five passages.

Generation of iPSC lines

Somatic reprogramming was used to generate control and aHUS iPSC lines from skin fibroblasts using the CytoTune-iPS 2.0 Sendai

Reprogramming Kit following the manufacturer's instructions (Life Technologies).

Differentiation of iPSC-ECs

The iPSCs were differentiated into ECs using a two-dimensional monolayer differentiation protocol as previously described (Tang et al., 2017). On day 0, iPSCs were placed in differentiation medium (RPMI and B-27 supplement minus insulin) (Gibco) with 6 μM CHIR-99021 (Axon Medchem) for 2 days, followed by differentiation medium with 3 μM CHIR-99021 for another 2 days. On day 4, the medium was changed to differentiation medium with 50 ng/mL VEGF (PeproTech) and 10 ng/mL basic fibroblast growth factor (PeproTech) for 5 days. On day 9, iPSC-ECs were sorted for CD144^{+} by MACS and cultured in EGM-2 medium (Lonza) on gelatin-coated plates.

Cell viability assay

The iPSC-ECs were cultured in 96-well plates. Cell analyses were performed using a CCK-8-based *in vitro* cell proliferation and cytotoxicity assay kit (Beyotime) according to the manufacturer's instructions. Cells were incubated with 10 μL of CCK-8 reagent per well for 12 h. Absorbance at 450 nm was measured using an iMark microplate reader (Bio-Rad).

TUNEL assay

We detected apoptosis by TUNEL assay using an In Situ Cell Death Detection Kit (Roche) in accordance with the manufacturer's instructions. iPSC-ECs were fixed with paraformaldehyde for 1 h, permeabilized with 0.2% Triton X-100, and incubated with TUNEL reaction mixture for 1 h. Images were collected and analyzed using a High Content Cell Imaging System (Operetta).

Wound-healing assay

The iPSC-ECs were seeded in one well of a 24-well plate overnight in EGM-2 medium. Cells were seeded at 300,000 per well in a 24-well plate overnight at 37°C in starvation medium without FBS to form a confluent cell monolayer. A linear scratch was generated by a sterile 200-μL plastic tip and cells were washed with DPBS, and EGM-2 medium with FBS was added to cells. Four representative images were collected from each well at 0 h and 12 h, and analyzed by ImageJ.

Tube formation assay

A volume of 200 μL of Matrigel was plated in one well of a 24-well plate and incubated for 30 min at 37°C. A total of 10×10^4 iPSC-ECs were seeded on Matrigel, and the formation of cord-like structures was assessed after 6 h. A total of 3–5 random fields in each well were imaged and counted under a 10× phase-contrast microscope (Olympus).

Cell proliferation assay

A cell proliferation assay was used to analyze the proliferation of ECs following the manufacturer's protocols (Cell Signaling Technology). The iPSC-ECs were incubated in EGM-2 medium along with bromodeoxyuridine solution for 6 h at 37°C. Horseradish peroxidase conjugate substrate was subsequently added, and the absorbance was read at 450 nm by MD M5 SpectraMax (Molecular Devices). All experiments were performed in triplicates, and data were analyzed using GraphPad Prism 6 (GraphPad Software).

Purification of total IgG

The total IgG was isolated using a Protein G affinity column (GE Healthcare, Freiburg, Germany) from the first plasma exchange fluid of aHUS patients #1 and #2 (aHUS#1 and aHUS#2), and plasma from a healthy control subject. Chromatography was performed according to the manufacturer's instructions. Samples were applied to a Protein G affinity column with 10 mM phosphate buffer/DPBS (pH 7.4) as the starting buffer and 0.1 mol/L glycine-HCl (pH 2.7) as the eluting buffer. Once the total IgG was eluted, the eluate was immediately neutralized to pH 7.0 using 10 mM Tris-HCl (pH 9.0), and thereafter was concentrated and dialyzed against DPBS.

Purification of anti-CFH autoantibodies

The total IgG amounts isolated from aHUS#1 and aHUS#2 were further applied to a CFH affinity column with 10 mM DPBS (pH 7.4) as the starting buffer and 10 mM glycine-HCl (pH 2.7) as the eluting buffer. Once the anti-CFH autoantibodies were eluted, the eluate was immediately neutralized to pH 7.0 using 0.01 mol/L Tris-HCl (pH 9.0), then concentrated and dialyzed against DPBS. The purified anti-CFH autoantibodies were confirmed by western blot and immunofixation electrophoresis assays. All proteins were stored at −70°C until analysis.

RNA sequencing

Total RNA was isolated and used for RNA-seq analysis. cDNA library construction and sequencing were performed at Beijing Genomics Institute using the BGISEQ-500 platform. High-quality reads were aligned to the human reference genome (GRCh38) using Bowtie2. The expression levels for each of the genes were normalized to fragments per kilobase of exon model per million mapped reads (FPKM) using RSEM (RNA-seq by the Expectation-Maximization algorithm). Differentially expressed genes were identified with a q value of ≤0.001 and a fold change of ≥2 between control and aHUS iPSC-derived cardiomyocytes.

Compounds and solutions

Sera from aHUS patients were provided by Peking University First Hospital. Both the normal and aHUS serums for EC stimulation were diluted with EGM-2 medium at a volume ratio of 1:3. Serum denaturation was processed under the condition of boiling at 56°C for 30 min, resulting in inactivated complements. The concentrations of normal IgG, anti-CFH autoantibody from aHUS patient #1 (aHUS#1), and anti-CFH autoantibody from aHUS patient #2 (aHUS#2) were 6 mg/mL, 4 μg/mL, and 12 μg/mL, respectively. ANS was purchased from Alomone Labs, and 10 mM stock solutions were prepared in dimethylsulfoxide (Sigma-Aldrich). Compstatin was purchased from Selleck, and 50 mM stock solutions were prepared in H_2O.

Statistical analysis

Statistical significance was determined by unpaired two-tailed Student's t test to compare two groups and by one-way ANOVA

to compare multiple groups. A p value of <0.05 was considered statistically significant. Data are shown as mean ± standard error of the mean and were analyzed by GraphPad Prism 6.

Data and code availability

The accession number for the RNA-seq data reported in this study is NCBI SRA: PRJNA563529.

SUPPLEMENTAL INFORMATION

Supplemental information can be found online at https://doi.org/10.1016/j.stemcr.2021.07.011.

AUTHOR CONTRIBUTIONS

F.Y., P.L., X.L., and M.Z. designed and supervised the study. D.Z., Y.T., X.L., L.T., H.W., J.S., W.W., L.Z., J.T., J.S. and T.G. performed the experiments and analyzed data. D.Z., Y.T., and P.L. wrote the manuscript.

CONFLICTS OF INTERESTS

The authors declare no competing interests.

REFERENCES

Barruet, E., Morales, B.M., Lwin, W., White, M.P., Theodoris, C.V., Kim, H., Urrutia, A., Wong, S.A., Srivastava, D., and Hsiao, E.C. (2016). The ACVR1 R206H mutation found in fibrodysplasia ossificans progressiva increases human induced pluripotent stem cell-derived endothelial cell formation and collagen production through BMP-mediated SMAD1/5/8 signaling. Stem Cell Res. Ther. 7, 115.

Blanc, C., Roumenina, L.T., Ashraf, Y., Hyvarinen, S., Sethi, S.K., Ranchin, B., Niaudet, P., Loirat, C., Gulati, A., Bagga, A., et al. (2012). Overall neutralization of complement factor H by autoan-tibodies in the acute phase of the autoimmune form of atypical hemolytic uremic syndrome. J. Immunol. 189, 3528–3537.

Bruneau, S., Neel, M., Roumenina, L.T., Frimat, M., Laurent, L., Fremeaux-Bacchi, V., and Fakhouri, F. (2015). Loss of DGKepsilon induces endothelial cell activation and death independently of complement activation. Blood 125, 1038–1046.

Caprioli, J., Noris, M., Brioschi, S., Pianetti, G., Castelletti, F., Bettinaglio, P., Mele, C., Bresin, E., Cassis, L., Gamba, S., et al. (2006). Genetics of HUS: the impact of MCP, CFH, and IF mutations on clinical presentation, response to treatment, and outcome. Blood 108, 1267–1279.

Chen, Y., Dawes, P.T., Packham, J.C., and Mattey, D.L. (2012). Interaction between smoking and functional polymorphism in the TGFB1 gene is associated with ischaemic heart disease and myocardial infarction in patients with rheumatoid arthritis: a cross-sectional study. Arthritis Res. Ther. 14, R81.

Corre, I., Paris, F., and Huot, J. (2017). The p38 pathway, a major pleiotropic cascade that transduces stress and metastatic signals in endothelial cells. Oncotarget 8, 55684–55714.

de Jorge, E.G., Macor, P., Paixão-Cavalcante, D., Rose, K.L., Tedesco, F., Cook, H.T., Botto, M., and Pickering, M.C. (2011). The development of atypical hemolytic uremic syndrome depends on complement C5. J. Am. Soc. Nephrol. 22, 137–145.

Dragon-Durey, M.A., Loirat, C., Cloarec, S., Macher, M.A., Blouin, J., Nivet, H., Weiss, L., Fridman, W.H., and Fremeaux-Bacchi, V. (2005). Anti-Factor H autoantibodies associated with atypical hemolytic uremic syndrome. J. Am. Soc. Nephrol. 16, 555–563.

Dragon-Durey, M.A., Sethi, S.K., Bagga, A., Blanc, C., Blouin, J., Ranchin, B., André, J.L., Takagi, N., Cheong, H.I., Hari, P., et al. (2010). Clinical features of anti-factor H autoantibody-associated hemolytic uremic syndrome. J. Am. Soc. Nephrol. 21, 2180–2187.

Durey, M.A., Sinha, A., Togarsimalemath, S.K., and Bagga, A. (2016). Anti-complement-factor H-associated glomerulopathies. Nat. Rev. Nephrol. 12, 563–578.

Feitz, W.J.C., van de Kar, N., Orth-Holler, D., van den Heuvel, L., and Licht, C. (2018). The genetics of atypical hemolytic uremic syndrome. Med. Genet. 30, 400–409.

Giannotta, M., Trani, M., and Dejana, E. (2013). VE-cadherin and endothelial adherens junctions: active guardians of vascular integrity. Dev. Cell 26, 441–454.

Gu, M., Shao, N.Y., Sa, S., Li, D., Termglinchan, V., Ameen, M., Karakikes, I., Sosa, G., Grubert, F., Lee, J., et al. (2017). Patient-specific iPSC-derived endothelial cells uncover pathways that protect against pulmonary hypertension in BMPR2 mutation carriers. Cell Stem Cell 20, 490–504 e495.

Guo, W.Y., Song, D., Liu, X.R., Chen, Z., Xiao, H.J., Ding, J., Sun, S.Z., Liu, H.Y., Wang, S.X., Yu, F., et al. (2019). Immunological features and functional analysis of anti-CFH autoantibodies in patients with atypical hemolytic uremic syndrome. Pediatr. Nephrol. 34, 269–281.

Hamauchi, S., Shichinohe, H., Uchino, H., Yamaguchi, S., Nakayama, N., Kazumata, K., Osanai, T., Abumiya, T., Houkin, K., and Era, T. (2016). Cellular functions and gene and protein expression profiles in endothelial cells derived from moyamoya disease-specific iPS cells. PLoS One 11, e0163561.

Hitomi, T., Habu, T., Kobayashi, H., Okuda, H., Harada, K.H., Osafune, K., Taura, D., Sone, M., Asaka, I., Ameku, T., et al. (2013). Downregulation of Securin by the variant RNF213 R4810K (rs112735431, G>A) reduces angiogenic activity of induced pluripotent stem cell-derived vascular endothelial cells from moyamoya patients. Biochem. Biophys. Res. Commun. 438, 13–19.

Hofer, J., Giner, T., and Safouh, H. (2014). Diagnosis and treatment of the hemolytic uremic syndrome disease spectrum in developing regions. Semin. Thromb. Hemost. 40, 478–486.

Ikeda, K., Mizoro, Y., Ameku, T., Nomiya, Y., Mae, S.I., Matsui, S., Kuchitsu, Y., Suzuki, C., Hamaoka-Okamoto, A., Yahata, T., et al. (2016). Transcriptional analysis of intravenous immunoglobulin resistance in Kawasaki disease using an induced pluripotent stem cell disease model. Circ. J. 81, 110–118.

Issbrucker, K., Marti, H.H., Hippenstiel, S., Springmann, G., Voswinckel, R., Gaumann, A., Breier, G., Drexler, H.C., Suttorp, N., and Clauss, M. (2003). p38 MAP kinase–a molecular switch between VEGF-induced angiogenesis and vascular hyperpermeability. FASEB J. 17, 262–264.

Józsi, M., Licht, C., Strobel, S., Zipfel, S.L., Richter, H., Heinen, S., Zipfel, P.F., and Skerka, C. (2008). Factor H autoantibodies in atypical hemolytic uremic syndrome correlate with CFHR1/CFHR3 deficiency. Blood 111, 1512–1514.

Jozsi, M., Strobel, S., Dahse, H.M., Liu, W.S., Hoyer, P.F., Oppermann, M., Skerka, C., and Zipfel, P.F. (2007). Anti factor H autoantibodies block C-terminal recognition function of factor H in hemolytic uremic syndrome. Blood 110, 1516–1518.

Kim, S.R., Lee, K.S., Park, S.J., Jeon, M.S., and Lee, Y.C. (2012). Inhibition of p38 MAPK reduces expression of vascular endothelial growth factor in allergic airway disease. J. Clin. Immunol. 32, 574–586.

Kumar, S., Boehm, J., and Lee, J.C. (2003). p38 MAP kinases: key signalling molecules as therapeutic targets for inflammatory diseases. Nat. Rev. Drug Discov. 2, 717–726.

Kuroyanagi, G., Tokuda, H., Yamamoto, N., Matsushima-Nishiwaki, R., Mizutani, J., Kozawa, O., and Otsuka, T. (2015). Resveratrol amplifies BMP-4-stimulated osteoprotegerin synthesis via p38 MAP kinase in osteoblasts. Mol. Med. Rep. 12, 3849–3854.

Lertkiatmongkol, P., Liao, D., Mei, H., Hu, Y., and Newman, P.J. (2016). Endothelial functions of platelet/endothelial cell adhesion molecule-1 (CD31). Curr. Opin. Hematol. 23, 253–259.

Lim, R.G., Quan, C., Reyes-Ortiz, A.M., Lutz, S.E., Kedaigle, A.J., Gipson, T.A., Wu, J., Vatine, G.D., Stocksdale, J., Casale, M.S., et al. (2017). Huntington's disease iPSC-derived brain microvascular endothelial cells reveal WNT-mediated angiogenic and blood-brain barrier deficits. Cell Rep. 19, 1365–1377.

Loirat, C., and Frémeaux-Bacchi, V. (2011). Atypical hemolytic uremic syndrome. Orphanet J. Rare Dis. 6, 60.

Loirat, C., Noris, M., and Fremeaux-Bacchi, V. (2008). Complement and the atypical hemolytic uremic syndrome in children. Pediatr. Nephrol. 23, 1957–1972.

Mamo, T.M., Wittern, A.B., Kleppa, M.J., Bohnenpoll, T., Weiss, A.C., and Kispert, A. (2017). BMP4 uses several different effector pathways to regulate proliferation and differentiation in the epithelial and mesenchymal tissue compartments of the developing mouse ureter. Hum. Mol. Genet. 26, 3553–3563.

McCarthy, N., Wetherill, L., Lovely, C.B., Swartz, M.E., Foroud, T.M., and Eberhart, J.K. (2013). Pdgfra protects against ethanol-induced craniofacial defects in a zebrafish model of FASD. Development 140, 3254–3265.

Noone, D., Waters, A., Pluthero, F.G., Geary, D.F., Kirschfink, M., Zipfel, P.F., and Licht, C. (2014). Successful treatment of DEAP-HUS with eculizumab. Pediatr. Nephrol. 29, 841–851.

Noris, M., Caprioli, J., Bresin, E., Mossali, C., Pianetti, G., Gamba, S., Daina, E., Fenili, C., Castelletti, F., Sorosina, A., et al. (2010). Relative role of genetic complement abnormalities in sporadic and familial aHUS and their impact on clinical phenotype. Clin. J. Am. Soc. Nephrol. 5, 1844–1859.

Noris, M., and Remuzzi, G. (2005). Hemolytic uremic syndrome. J. Am. Soc. Nephrol. 16, 1035–1050.

Noris, M., and Remuzzi, G. (2009). Atypical hemolytic-uremic syndrome. N. Engl. J. Med. 361, 1676–1687.

Ong, S.B., Lee, W.H., Shao, N.Y., Ismail, N.I., Katwadi, K., Lim, M.M., Kwek, X.Y., Michel, N.A., Li, J., Newson, J., et al. (2019). Calpain inhibition restores autophagy and prevents mitochondrial fragmentation in a human iPSC model of diabetic endotheliopathy. Stem Cell Rep. 12, 597–610.

Puraswani, M., Khandelwal, P., Saini, H., Saini, S., Gurjar, B.S., Sinha, A., Shende, R.P., Maiti, T.K., Singh, A.K., Kanga, U., et al. (2019). Clinical and immunological profile of anti-factor H antibody associated atypical hemolytic uremic syndrome: a nationwide database. Front. Immunol. 10, 1282.

Raina, R., Krishnappa, V., Blaha, T., Kann, T., Hein, W., Burke, L., and Bagga, A. (2019). Atypical hemolytic-uremic syndrome: an update on pathophysiology, diagnosis, and treatment. Ther. Apher. Dial. 23, 4–21.

Rezzola, S., Di Somma, M., Corsini, M., Leali, D., Ravelli, C., Polli, V.A.B., Grillo, E., Presta, M., and Mitola, S. (2019). VEGFR2 activation mediates the pro-angiogenic activity of BMP4. Angiogenesis 22, 521–533.

Rossi, S., Motta, C., Studer, V., Monteleone, F., De Chiara, V., Buttari, F., Barbieri, F., Bernardi, G., Battistini, L., Cutter, G., et al. (2013). A genetic variant of the anti-apoptotic protein Akt predicts natalizumab-induced lymphocytosis and post-natalizumab multiple sclerosis reactivation. Mult. Scler. 19, 59–68.

Sa, S., Gu, M., Chappell, J., Shao, N.Y., Ameen, M., Elliott, K.A., Li, D., Grubert, F., Li, C.G., Taylor, S., et al. (2017). Induced pluripotent stem cell model of pulmonary arterial hypertension reveals novel gene expression and patient specificity. Am. J. Respir. Crit. Care Med. 195, 930–941.

Saklatvala, J. (2004). The p38 MAP kinase pathway as a therapeutic target in inflammatory disease. Curr. Opin. Pharmacol. 4, 372–377.

Seikrit, C., Ronco, P., and Debiec, H. (2018). Factor H autoantibodies and membranous nephropathy. N. Engl. J. Med. 379, 2479–2481.

Shi, Y., Inoue, H., Wu, J.C., and Yamanaka, S. (2017). Induced pluripotent stem cell technology: a decade of progress. Nat. Rev. Drug Discov. 16, 115–130.

Sinha, A., Gulati, A., Saini, S., Blanc, C., Gupta, A., Gurjar, B.S., Saini, H., Kotresh, S.T., Ali, U., Bhatia, D., et al. (2014). Prompt plasma exchanges and immunosuppressive treatment improves the outcomes of anti-factor H autoantibody-associated hemolytic uremic syndrome in children. Kidney Int. 85, 1151–1160.

Smith-Jackson, K., Yang, Y., Denton, H., Pappworth, I.Y., Cooke, K., Barlow, P.N., Atkinson, J.P., Liszewski, M.K., Pickering, M.C., Kavanagh, D., et al. (2019). Hyperfunctional complement C3 promotes C5-dependent atypical hemolytic uremic syndrome in mice. J. Clin. Invest. 129, 1061–1075.

Song, D., Liu, X.R., Chen, Z., Xiao, H.J., Ding, J., Sun, S.Z., Liu, H.Y., Guo, W.Y., Wang, S.X., Yu, F., et al. (2017). The clinical and laboratory features of Chinese Han anti-factor H autoantibody-associated hemolytic uremic syndrome. Pediatr. Nephrol. 32, 811–822.

Strippoli, R., Benedicto, I., Foronda, M., Perez-Lozano, M.L., Sanchez-Perales, S., Lopez-Cabrera, M., and Del Pozo, M.A. (2010). p38 maintains E-cadherin expression by modulating TAK1-NF-kappa B during epithelial-to-mesenchymal transition. J. Cell Sci. 123, 4321–4331.

Strobel, S., Abarrategui-Garrido, C., Fariza-Requejo, E., Seeberger, H., Sanchez-Corral, P., and Jozsi, M. (2011). Factor H-related protein 1 neutralizes anti-factor H autoantibodies in autoimmune hemolytic uremic syndrome. Kidney Int. 80, 397–404.

Strobel, S., Hoyer, P.F., Mache, C.J., Sulyok, E., Liu, W.S., Richter, H., Oppermann, M., Zipfel, P.F., and Józsi, M. (2010). Functional analyses indicate a pathogenic role of factor H autoantibodies in atypical haemolytic uraemic syndrome. Nephrol. Dial. Transpl. 25, 136–144.

Takahashi, K., Tanabe, K., Ohnuki, M., Narita, M., Ichisaka, T., Tomoda, K., and Yamanaka, S. (2007). Induction of pluripotent stem cells from adult human fibroblasts by defined factors. Cell 131, 861–872.

Tang, L., Su, J., and Liang, P. (2017). Modeling cadmium-induced endothelial toxicity using human pluripotent stem cell-derived endothelial cells. Sci. Rep. 7, 14811.

Tielemans, B., Stoian, L., Gijsbers, R., Michiels, A., Wagenaar, A., Farre Marti, R., Belge, C., Delcroix, M., and Quarck, R. (2019). Cytokines trigger disruption of endothelium barrier function and p38 MAP kinase activation in BMPR2-silenced human lung microvascular endothelial cells. Pulm. Circ. 9, 2045894019883607.

Ueda, Y., Mohammed, I., Song, D., Gullipalli, D., Zhou, L., Sato, S., Wang, Y., Gupta, S., Cheng, Z., Wang, H., et al. (2017). Murine systemic thrombophilia and hemolytic uremic syndrome from a factor H point mutation. Blood 129, 1184–1196.

Yong, H.Y., Koh, M.S., and Moon, A. (2009). The p38 MAPK inhibitors for the treatment of inflammatory diseases and cancer. Expert Opin. Invest. Drugs 18, 1893–1905.